ACS OMEGA

Open Access

http://pubs.acs.org/journal/acsodf

Article

Solubility and Mass Transfer Performance of Ethane and *n*-Butane in Menthol and Decanoic Acid Deep Eutectic Solvent

Yunfei Song*

Cite This: *ACS Omega* 2024, 9, 30935−30944

Read Online

ACCESS | Metrics & More | Article Recommendations | Supporting Information

ABSTRACT: The absorption performance and mechanism of the deep eutectic solvent (DES), composed of menthol and decanoic acid, were investigated. The solubility of volatile organic compounds (VOCs) in the DES was studied through saturation solution experiments, wherein the solubility of ethane and *n*-butane increases with a decrease in temperature and increasing pressure. Henry's law constants of ethane and *n*-butane in the DES at 288.2 K were 2.089 and 0.136 MPa, respectively, demonstrating the high solubility for light hydrocarbons that surpasses or equals that of ionic liquids. The mass transfer and regeneration performance of the DES were investigated by using dynamic bubbling experiments. Results demonstrated that the removal rate of both ethane and *n*-butane increased as the gas flow rate decreased and the VOC concentration in the model gas increased. Specifically, the removal rate of ethane reached 99.50% at a temperature of 293.2 K, a VOC concentration VOC of 10,000 μmol/mol, and a gas flow rate of 30 mL/min, while the removal rate of *n*-butane was higher than that of ethane under the same conditions, achieving a removal rate exceeding 99.99%. Furthermore, no significant decrease in the removal rate for *n*-butane was observed during the four regeneration processes. Interaction energies between the VOC molecule and DES were calculated using the quantum chemistry method. It was found that the interactions between the VOC molecule and DES are primarily attributed to dispersion attractive effects which belong to weak interactions; therefore, the absorption of light hydrocarbon by the DES belongs to a physical process. The DES has been proven to be effective for the recovery of light hydrocarbons, providing a promising approach to address the key challenge in comprehensive treatment of VOCs in the petrochemical industry.

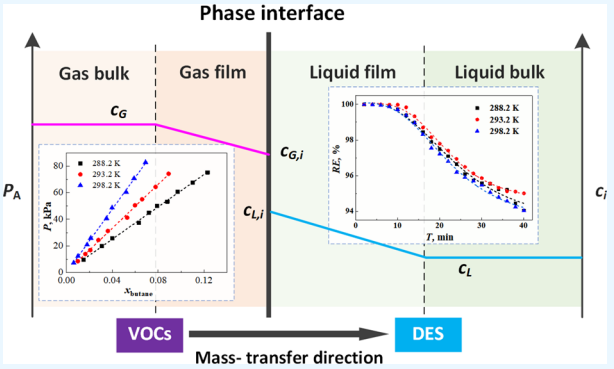

1. INTRODUCTION

Volatile organic compounds (VOCs) are key precursors of ozone and fine particulate matter (PM), which pose serious hazards to the environment and human health. In recent years, the rapid development of industry has led to an increasing concentration and total amount of VOC emissions, resulting in VOCs being recognized as the second major type of atmospheric pollutants in terms of quantity and distribution after PM.[1] Therefore, VOC treatment has emerged as a prominent research area within the field of environmental protection for a long time. The storage, transportation, sales, and refining processes involved in gasoline, diesel, and other oil products result in high concentrations of VOC emissions. Constructing VOC recovery devices can effectively mitigate air pollution caused by VOC volatilization while simultaneously enhancing resource utilization. The common VOC recovery technologies include adsorption, condensation, membrane separation, and absorption.[2−5] The industrial sector commonly employs various technology combinations, such as adsorption-thermal oxidation, absorption-adsorption, condensation-adsorption, and membrane separation-adsorption, to achieve a recovery efficiency of over 95% for components above C4.[6] However, conventional VOC recovery methods face challenges in efficiently removing light hydrocarbons like C2−C4 due to their stable properties, making them difficult to liquefy or enrich.[7,8] Developing efficient technology for recovering C2−C4 light hydrocarbon VOCs and improving overall nonmethane hydrocarbon recovery[9] are crucial issues toward achieving deep reductions in VOC emissions.

The absorption technology is a gas recovery method that involves dissolving gas in an absorbent, making it suitable for handling high-volume gas streams. This approach offers several advantages, including a well-established process, lower investment requirements, and simplified equipment operation and maintenance.[10,11] Diesel and low-temperature gasoline are commonly employed as oil and gas absorbents in the industrial

Received: April 23, 2024
Revised: June 19, 2024
Accepted: June 21, 2024
Published: July 2, 2024

sector. However, due to the high volatility of gasoline and diesel, achieving comprehensive treatment of VOCs through conventional absorption processes poses challenges. The development of novel absorbents with reduced volatility and enhanced absorption efficiency is instrumental in overcoming the technical limitations associated with absorption technology for VOC treatment.

In recent years, the application of ionic liquids (ILs) in the field of VOC absorption has attracted widespread attention because of their excellent performance as absorbents, such as extremely low vapor pressure, nonflammability, good stability, and functional design, for the recovery of different VOCs.[12−15] In the absorption of light hydrocarbon VOCs, increasing the nonpolarity of ILs (such as increasing the length of anionic and cationic alkyl chains) can improve the solubility of light hydrocarbons in ILs.[16,17] According to Liu's experimental results, the Henry coefficients of ethane in [P4444][TMPP] and [P666,14][TMPP] ILs at 313.2 K were 5.49 MPa[18] and 1.90 MPa,[19] respectively. Makino studied the solubility of *n*-butane in ILs and found that the maximum mole fraction of *n*-butane in [P666,14][AOT] IL at 298.2 K and 0.101 MPa was approximately 0.48. However, the viscosity of [P666,14]-[TMPP] and [P666,14][AOT] ILs at 298.2 K was as high as 1004 mPa s[20] and 1431 mPa s,[21] respectively. High viscosity results in poor mass transfer performance of light hydrocarbons in ILs. In addition, the potential toxicity, complex preparation process, and high cost of ILs also limit their industrial promotion.

As a new type of green solvent, deep eutectic solvents (DESs)[22] are liquid mixtures formed by hydrogen bond donors (such as alcohols, organic acids, amides, etc.) and hydrogen bond acceptors (such as quaternary ammonium/phosphorus salts, terpenes, etc.) through intermolecular hydrogen bonding. The properties of DESs are similar to those of ILs but more environmentally friendly and cost-effective. Therefore, DESs are considered to be promising alternative solvents for both organic solvents and ILs.

The feasibility of DESs as absorbents has been confirmed in the fields of CO_2 capture[23−25] and acid/base gas treatment.[26−28] However, relevant research in the field of VOC treatment is still in its infancy. Moura[29] conducted relevant exploratory work in 2017, which verified that the absorption performance, in terms of absorption capacity and cycling performance, of quaternary ammonium salt DESs for toluene, acetaldehyde, and dichloromethane is comparable to that of imidazolium ILs and silicone oil. Słupek[30] proposed that the chlorinated choline-tetraethylene glycol 1:2 DES can effectively remove toluene impurities from biogas, and its dynamic absorption performance is higher than that of imidazolium ILs. Song et al.[31] studied the absorption performance of hydrophobic DES tetraethylammonium chloride-oleic acid (1:3) for toluene. The results showed that toluene can be effectively captured by the DES, and the structure and composition of the DES have significant impacts on its absorption performance. Moufawad et al.[32] determined the absorption performance of various VOCs such as toluene and *n*-heptane in DESs and found that the DES did not reach absorption saturation even at high VOC concentrations; moreover, the absorption capacity of the tetrabutylammonium bromide-decanoic acid (1:2) DES for toluene and *n*-heptane at 30 °C was 280 and 8000 times that of water, respectively.

The above studies have demonstrated the feasibility of DESs as absorbents for VOC recovery, and their absorption capacity and dynamic absorption performance can reach the same level as conventional organic solvents and ILs. However, the viscosity of most DESs is relatively high, which is not conducive to mass transfer. Chen[33] found that molecular hydrophobic eutectic solvents have lower viscosity, among which the low-viscosity DES prepared by menthol and decanoic acid in a molar ratio of 1:2 has a viscosity of 27.3 mPa s and a density of 0.89 kg m^{-3} at 298.2 K,[34] which can effectively improve the mass transfer performance during absorption process. However, the absorption performance and mechanism of this low-viscosity DES for light hydrocarbons have not been reported yet.

This work selects low-viscosity DES menthol-capric acid (1:2) as the absorbent. The ethane and *n*-butane were chosen as the research objective because the recovery of ethane poses the greatest challenge, whereas butane exhibits the highest concentration among other light hydrocarbons. First, the solubility of ethane and *n*-butane in the DES was investigated by steady-state solubility experiments. Besides, the dynamic bubble absorption experiments were performed to investigate the mass transfer performance of the DES and factors including absorption temperature, VOC concentration in the model gas (consisting of hydrocarbon VOCs and nitrogen), model gas flow rate, and regeneration performance. Moreover, the molecular interaction energy was calculated and analyzed to reveal the mechanism for the absorption of ethane and *n*-butane by the DES. This work presents a promising novel approach aimed at addressing the key issue associated with the efficiency of light hydrocarbons and the comprehensive treatment of VOCs in the petrochemical industry.

2. EXPERIMENTS

2.1. Chemicals and Apparatus. Chemicals used were ethane, *n*-butane, nitrogen, DL-menthol, and decanoic acid; more details are given in Table 1. All the chemicals were used directly without further purification.

Table 1. Detailed Information of Chemicals

name	formula	CAS	mass fraction (%)	source
DL-menthol	$C_{10}H_{20}O$	89-78-1	98.0	Macklin Biotechnology Co., Ltd.
decanoic acid	$C_{10}H_{20}O_2$	334-48-5	98.0	Macklin Biotechnology Co., Ltd.
ethane	C_2H_6	74-84-0	99.99	Ludong Gas Expert Co., Ltd.
n-butane	C_4H_{10}	106-97-8	99.99	Ludong Gas Expert Co., Ltd.
nitrogen	N_2	7727-37-9	99.999	Ludong Gas Expert Co., Ltd.

Apparatus involved were electronic balance, Nanjing Bonita Scientific Instrument Co., Ltd., with an accuracy of ±0.01 g; pressure transmitter (0−100 kPa, absolute pressure), WIKA Automation Instrument (Suzhou) Co., Ltd., with an accuracy of 0.5%; and portable nonmethane total hydrocarbon analyzer (Focused Photonics Inc., EXPEC 3200), with nitrogen as the carrier gas, sampling period of 2 min.

2.2. Solubility Experiments. The experimental apparatus used for the solubility experiment is shown in Figure 1.

Details of solubility experiments are shown as follows:

1. Preparation of the DES. The DES was prepared using the same method as mentioned in the work of Chen et al.,[33] in

https://doi.org/10.1021/acsomega.4c03895
ACS Omega 2024, 9, 30935−30944

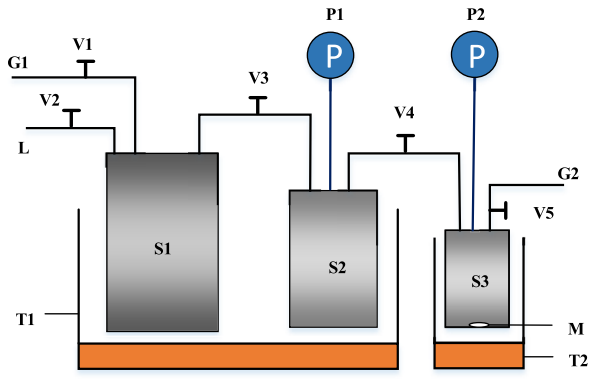

Figure 1. Apparatus for the solubility experiment. G1, G2: vacuum pump, V1 ~ V5: needle valve, P1, P2: digital pressure gauge, S1: gas bag of light hydrocarbon, S2: gas storage vessel, S3: absorption vessel, M: magnetic stirrer, T1, T2: thermostat bath.

which DL-menthol and decanoic acid were mixed at a molar ratio of 1:2 and heated at 333.2 K until a homogeneous liquid was formed and then cooled naturally. The water content was determined by Karl Fisher titration, which is 0.89 wt %.

2. Air tightness check of the device. The device undergoes an air tightness check by degassing it through the vacuum pump, followed by closing all valves. If the pressure change is below 0.1 kPa for more than 6 h, the device is deemed to be airtight.
3. Introducing the DES into the absorption vessel. The DES was measured by an analytical balance and introduced into S3.
4. Device degassing. The valves V2 and V5 were closed, and vacuum pump G1 was used to perform three rounds of degassing on the entire device through valve V1. Then close valve V1, open vacuum pump G2, and conduct an additional three rounds of degassing through valve V5 to remove air from the device.
5. VOC absorption. When the set temperature was achieved, the gas was introduced into S2 through V3 until reaching the predetermined pressure. Subsequently, valve V3 was closed and V4 was opened. As the gas dissolved in the DES in S3, there was a decrease in pressure within both S2 and S3. Once P2 and P3 remain stable for more than 60 min, it can be inferred that VOCs of light hydrocarbons have reached absorption equilibrium in the DES.

The solubility experiments of ethane and *n*-butane in the DES were performed at temperatures of 288.2, 293.2, and 298.2 K. Since the solubility experiment is performed in low pressure range, and the concentration of VOCs in the DES is quite low, it is assumed in this work that[35−37] (1) the gas behaves ideally; (2) negligible changes occur in the density and volume of the DES during the absorption process at the same temperature. By measuring pressure variations before and after light hydrocarbon absorption in the DES at different temperatures, it becomes possible to calculate the equilibrium content of the VOCs in the absorbent. n_A, the absorption capacity of light hydrocarbons, can be calculated by the ideal gas equation as shown in eq 1.

$$n_A = \frac{P^0 V_S - P^1 V_S - P(V_A - V_L)}{RT} \quad (1)$$

$$V_L = \frac{m}{\rho_T} \quad (2)$$

where V_S, V_A, and V_L represent the volume of the gas storage vessel, absorption vessel, and DES, respectively, m^3. P^0, P^1, and P are the initial pressure of the gas storage vessel, the equilibrium pressure of the gas storage vessel, and the equilibrium pressure of the absorption vessel, respectively, kPa. R is the thermodynamic constant, 8.314 J $mol^{-1}\cdot K^{-1}$. T is the experimental temperature, K. m is the mass of the DES in the absorption vessel, kg. ρ_T is the density of the DES at the experimental temperature, $kg\cdot m^{-3}$.

x, the equilibrium constant of VOCs, can be obtained by eq 3.

$$x = \frac{n_A}{n_A + n_L} \quad (3)$$

in which n_L and n_A are the amount of the DES and the light hydrocarbons dissolved in the DES, mol.

2.3. Dynamic Absorption Experiments. The device for dynamic bubbling experiments is shown in Figure 2.

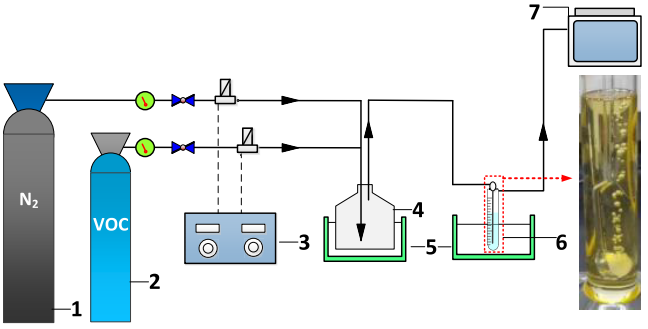

Figure 2. Dynamic absorption experiment device. 1, N_2; 2, VOC; 3, mass flow controller; 4, gas distributing vessel; 5, thermostat bath; 6, bubbling absorption device; 7, portable nonmethane total hydrocarbon analyzer.

Details of the experiments are shown as follows:

(1) Methods of dynamic bubbling experiments

The DES was introduced into the bubbling absorption device. A predetermined concentration of the VOC model gas was prepared using a mass flowmeter, and the portable nonmethane total hydrocarbon analyzer detected the VOC concentration in the model gas emitted from the buffer tank. Once the VOC concentration in the model gas maintained stability for 5 min at the set value, it indicated that the concentration of model gas in the buffer tank had stabilized. When the set absorption temperature was achieved, the model gas was introduced into the bubbling absorption device, and the outlet purified gas was analyzed by the portable nonmethane total hydrocarbon analyzer.

The experiment conditions are listed in Table 2.

(2) Methods of the regeneration of the DES

The solubility device was used for the regeneration of the DES under vacuum (with an absolute pressure of less than 5 kPa) and stirred for 30 min at 333.2 K.

In the absorption process, the mass transfer rate J can be expressed by eq 4.

$$dJ = F_G dc_G = K_L a^0 (c_L^* - c_L) dV \quad (4)$$

where F_G is the flow rate of the VOC model gas, $m^3\cdot s^{-1}$; c_G is the actual concentration of VOCs in the gas phase, $mol\cdot m^{-3}$; c_L and c_L^* are the actual and equilibrium concentrations of VOCs in the

https://doi.org/10.1021/acsomega.4c03895
ACS Omega 2024, 9, 30935−30944

Table 2. Dynamic Absorption Experiment Conditions

no.	c_{in} (μmol/mol)	F (mL/min)	temperature (K)	V_{DES} (mL)	regeneration times
1	10,000	30	288.2, 293.2, 298.2	130	
2	8000, 9000, 10,000	30	288.2	130	
3	10,000	30, 50, 100, 500	288.2	130	
4	10,000	30	288.2	130	3

liquid phase, mol·m^{-3}; K_La^0 is the mass transfer coefficient, s^{-1}; V is the volume of absorbent, m^3.

c_L^* can be calculated by Henry's law. Based on Biard's method,[38] both sides of eq 4 are integrated and the mass transfer coefficient equation can be obtained:

$$F_G(c_G - c_{G,0}) = \frac{K_La^0V}{K}\frac{(c_G - c_{G,0})}{\ln(c_G/c_{G,0})} \tag{5}$$

$$c_{G,0} = c_G\exp\left(-\frac{K_La^0V}{F_GH}\right) \tag{6}$$

in which, $c_{G,0}$ is the concentration of VOCs in the device outlet when the first bubble passes through the absorbent, mol·m^{-3}; K is the equilibrium constant; H is Henry's law constant.

As the time for the first bubble passing through the absorbent in the bubble device is quite short, the concentration of VOCs at the outlet at the absorption time $t = 0$ can be approximated as $c_{G,0}$, which will be determined by fitting the dynamic absorption data in this work. Then the mass transfer coefficient can be calculated by eq 6.

3. MOLECULAR INTERACTION ENERGY

The molecular interactions[31,39,40] between light hydrocarbon molecules and DES were analyzed by quantum chemical calculations with the ORCA 5.0[41] program first. The B97-3c method[42] was employed for the geometric structure optimizations, and the wB97M-V/def2-TZVP level was used for interaction energy ΔE by eq 7.

$$\Delta E = E_{AB}^{AB}(AB) - E_A^A(A) - E_B^B(B) - [E_A^{AB}(AB) - E_A^B(AB) + E_B^{AB}(AB) - E_B^B(AB)] \tag{7}$$

where $E_X^Y(Z)$ stands for the interaction energy for fragment X calculated at the optimized structure of fragment Y with the basis set of fragment Z.

Meanwhile, the Multiwfn 3.8 program[43] was utilized to perform energy decomposition based on AMBER force field analysis, which could decompose molecular interaction energy into electrostatic interactions and van der Waals forces, and the latter were further divided into exchange repulsion effects and dispersion attractions.

Within the framework of the AMBER force field, these energy decomposition terms were calculated as potentials by eqs 8−11.

$$E_{AB}^{ele} = \frac{q_Aq_B}{r_{AB}} \tag{8}$$

$$E_{AB}^{vdW} = E_{AB}^{rep} + E_{AB}^{disp} \tag{9}$$

$$E_{AB}^{rep} = \varepsilon_{AB}\left(\frac{R_{AB}^0}{r_{AB}}\right)^{12} \tag{10}$$

$$E_{AB}^{disp} = -2\varepsilon_{AB}\left(\frac{R_{AB}^0}{r_{AB}}\right)^{6} \tag{11}$$

where the subscripts A and B represent the defined interacting molecules; the superscripts ele, vdW, rep, and disp denote electrostatic interaction, van der Waals force, exchange repulsion, and dispersion attraction, respectively. The atomic charge q is measured in atomic units (a.u.), with Merz−Kollman (M−K) charge being adopted here. The interatomic distance r is measured in angstroms (Å), while ε represents the depth of the van der Waals potential well. R^0 denotes the nonbond distance between atoms in angstroms (Å), which is obtained by summing up the nonbond radii of atoms A and B according to the AMBER force field. When R^0 equals r, E^{vdW} is equal to ε.

4. RESULTS AND DISCUSSION

4.1. Solubility Experiments. The solubility experiments (Table S1) of ethane and n-butane in the DES were performed. Figure 3 and Table S2 illustrate the equilibrium pressure and liquid phase composition of light hydrocarbons. It can be observed that the solubility of ethane and n-butane in the DES decreases with rising temperature at the same pressure. Similarly, at a constant temperature, there is a significant

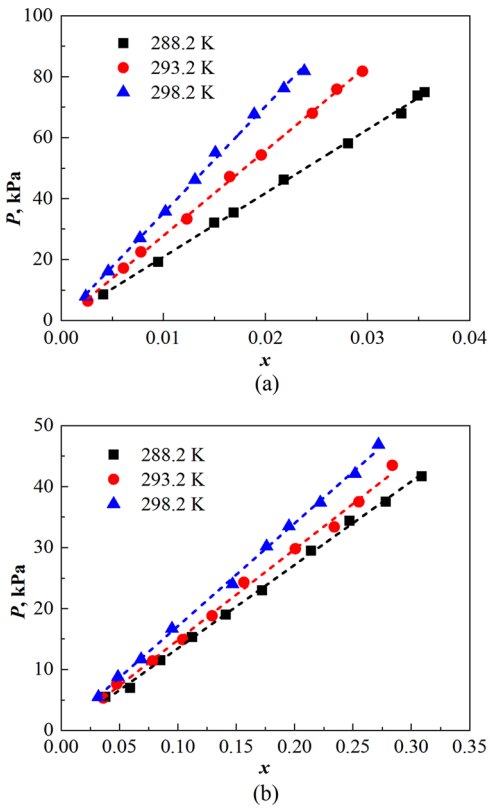

Figure 3. Solubility of (a) ethane and (b) n-butane in the DES at different pressures and temperatures.

https://doi.org/10.1021/acsomega.4c03895
ACS Omega 2024, 9, 30935−30944

increase in the solubility of light hydrocarbons as pressure rises. This phenomenon can be attributed to the exothermic process involved in weak molecular interactions between VOC molecules and the DES during absorption. Based on the kinetic-molecular theory,[44] as the temperature increases, more energy is provided to enhance molecular movement which disrupts the weak molecular interactions formed between VOCs and DES, so the gas escaping from the absorbent leads to decreased solubility. Conversely, an increase in pressure allows more gas molecules to enter into the liquid phase, thereby increasing solubility, and vice versa. In conclusion, lower absorption temperatures and higher absorption pressures are found to facilitate better absorption of ethane and *n*-butane in the DES.

Henry's law constant serves as an indicator for assessing the solubility of gases in the absorbent. A higher value of Henry's law constant corresponds to a lower value of gas solubility. Based on Henry's law, the equilibrium partial pressure of a gas is directly proportional to its molar composition in the dilute solution systems, and the proportionality factor is known as the composition-based Henry's law constant H, represented by eq 12.[35]

$$H = \frac{dP}{dx} \tag{12}$$

where P is the equilibrium partial pressure of the gas, KPa; x is the molar composition of the gas in the liquid phase.

The solubility data of ethane and *n*-butane were subjected to linear regression analysis (Table S2), and the resulting Henry's law constants are presented in Table 3.

Table 3. Henry's Law Constant

	H (MPa)	
temperature (K)	ethane	*n*-butane
288.2	2.089	0.136
293.2	2.791	0.149
298.2	3.538	0.169

As illustrated in Table 2, Henry's law constants of ethane in the DES have reached a level equivalent to that of the quaternary phosphate IL.[17−19] It can be calculated that the saturated molar fraction of *n*-butane in the DES at 298.2 K and 0.101 MPa is approximately 0.599, which exceeds the absorption capacity of the IL by more than 20%.[20] The higher solubility of light hydrocarbons in the DES is possibly due to the molecular nature of the molecular-type DES containing weakly polar functional groups such as alkyl, cycloalkyl, and carbon−oxygen double bonds, making the DES less polar than ILs. Therefore, based on the "like dissolves like" rule, more *n*-butane molecules were captured by the DES in this work. Furthermore, as the temperature decreases, the Henry coefficient decreases while solubility gradually increases. At 288.2 K and 0.101 MPa, the saturated molar fraction of *n*-butane is about 0.742. The results demonstrate that the menthol-decanoic acid 1:2 DES exhibits a significantly enhanced absorption capacity.

4.2. Dynamic Absorption Experiments. In dynamic absorption experiments, the influences of temperature, concentration of VOC in the model gas (consisting of N_2 and VOC), flow of the model gas, and regeneration times on the absorption efficiency have been investigated. The absorption efficiency can be expressed by the removal rate of VOC *RE* (eq 13).

$$RE = \frac{c_{in} - c_{out}}{c_{in}} \times 100\% \tag{13}$$

where c_{in} and c_{out} are the concentrations of VOC in the inlet and outlet, respectively, μmol/mol.

4.2.1. Influence of Temperature. The temperature exerts dual effects on the dynamic absorption efficiency. On the one hand, elevated temperatures result in a reduction of gas solubility in the DES, thereby diminishing the driving force for mass transfer and dynamic absorption efficiency. On the other hand, increased temperatures accelerate molecular motion and diffusion rates, which favor dynamic absorption.

The dynamic absorption results of ethane and *n*-butane model gases in the DES under different temperatures are presented in Figure 4 and Table S3. The results illustrate that with different

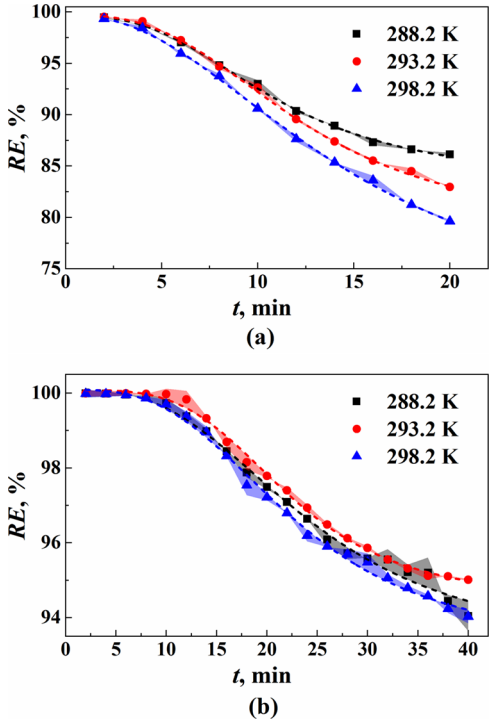

Figure 4. Removal rate of (a) ethane and (b) *n*-butane in the DES at different temperatures

absorption temperatures, the removal rate of ethane at the outlet of the device is the highest at 293.2 K in the first 6 min, while the highest at 288.2 K in the later 14 min. This proves that the acceleration of molecular motion and diffusion rates is significant with temperature increasing from 288.2 to 293.2 K at the beginning of the dynamic absorption process, while the decrease in solubility has a more pronounced impact in the later 14 min. With the temperature increasing from 293.2 to 298.2 K, the removal rate decreases, which demonstrates that the dominant factor affecting dynamic absorption efficiency is the reduction of solubility in this process. For *n*-butane, the overall *n*-butane removal rate is the highest at 293.2 K, followed by 288.2 K, and the lowest at 298.2 K.

The nonlinear function with the orthogonal distance regression algorithm was employed to fit the experimental data of the dynamic removal rate (eq 14 and Table S4). The point of intersection between the fitting curve and the vertical axis represented the ethane removal rate at $t = 0$, serving as a basis for calculating $c_{G,0}$. The mass transfer coefficient $K_L a^0$ and

https://doi.org/10.1021/acsomega.4c03895
ACS Omega 2024, 9, 30935−30944

Table 4. Mass Transfer Coefficient K_La^0 and Initial Mass Transfer Rate J_0 of Ethane and *n*-Butane in the DES at Different Temperatures

	ethane			*n*-butane		
T (K)	$K_La^0/10^{-3}$ s^{-1}	$J_0/10^{-4}$ mol s^{-1}	R^2	$K_La^0/10^{-3}$ s^{-1}	$J_0/10^{-4}$ mol s^{-1}	R^2
288.2	17.34	1.98	0.995	1.71	3.00	0.997
293.2	25.32	2.20	0.995	2.09	3.41	0.997
298.2	31.54	2.23	0.996	1.87	2.75	0.995

mass transfer rate J_0 of VOCs in the DES at $t = 0$ are presented in Table 4. It can be seen that the mass transfer coefficient of ethane in the DES is higher than that of *n*-butane due to the lower diffusion resistance caused by its smaller molecular size.[45] Additionally, the initial absorption rate of *n*-butane is higher because *n*-butane has greater solubility in the DES, which provides a larger concentration gradient resulting in a higher equilibrium concentration. Considering the temperature, the mass transfer coefficient and initial absorption rate increase with the temperature rise for ethane, which demonstrates that the proper elevation of temperature facilitates efficient mass transfer for ethane. While for *n*-butane, the values of both the mass transfer coefficient and initial absorption rate at 293.2 K are higher than those at 288.2 and 298.2 K. That is the mass transfer coefficient and initial absorption rate for *n*-butane exhibited a trend of initially increasing and then decreasing with the temperature rising from 288.2 to 298.2 K. Based on the fitting results, it was found that at an initial time, the *n*-butane removal rate at the outlet of the device exceeded 99.99% when operating at 293.2 K.

$$y = b + [a - b)/(1 + (x/x_0)^p] \quad (14)$$

4.2.2. Influence of Concentration of VOC in the Model Gas. The removal rates of ethane and *n*-butane and VOC concentrations of the model gas for different VOC concentrations of the model gas are presented in Figure 5 and Table S5. The results indicate a decrease in the removal rate of both ethane and *n*-butane with increasing absorption time. According to the double film theory,[46] the mass transfer rate during gas absorption is influenced by molecular diffusion in both the gas and liquid film regions, where the concentration gradient between the phase interface and bulk solution serves as the driving force for molecular diffusion. There is a gradual increase in gas concentration within the absorbent as absorption progresses, leading to a reduction in mass transfer driving force and subsequently decreasing the gas removal rate over time. Additionally, it can be observed that as the VOC concentration decreases in the model gas, so does its concentration at the device outlet. However, the dynamic removal rate exhibits an opposite trend. This discrepancy arises from an increase in partial pressure of VOCs on the gas film side when the VOC content rises within the model gas, which enhances the concentration gradient between phases and improves the mass transfer driving force, resulting in an increased ethane removal rate.[47] The mass transfer coefficient and initial mass transfer rate of VOCs in the DES were calculated and are shown in Table 5, and the fitting results are shown in Table S6. It reveals that as the VOC concentration in the model gas increases, both the mass transfer coefficient and initial mass transfer rate exhibit a slightly upward trend. This is also attributed to the fact that a higher VOC concentration results in a steeper concentration gradient, thereby facilitating mass transfer.

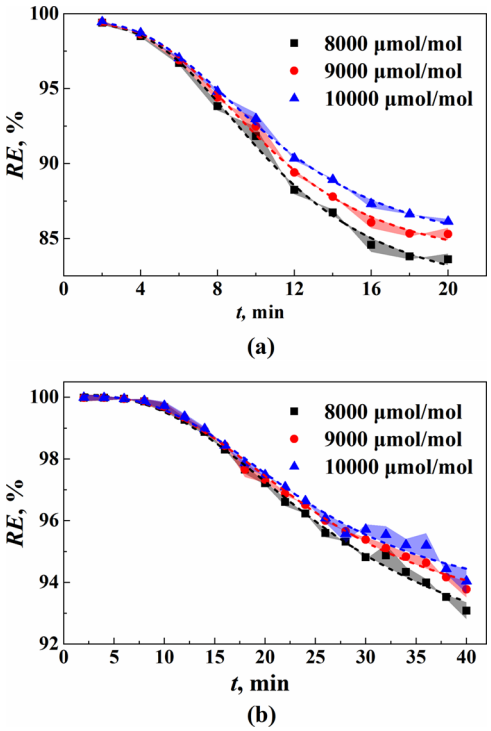

Figure 5. Removal rate of (a) ethane and (b) *n*-butane in the DES at different VOC concentrations.

4.2.3. Influence of Flow Rate of the Model Gas. Figure 6 and Table S7 demonstrate the dynamic absorption effect of the DES on ethane and *n*-butane with different flow rates of the model gas. The results indicate that as the flow rate decreases, the VOC concentration at the device outlet significantly decreases, while the overall removal rate increases. This can be attributed to a shorter residence time of the gas in the liquid phase with higher model gas flow rates, resulting in some VOC molecules being carried out of the absorbent with the flow without passing through the gas–liquid interface into the liquid phase. In other words, an increase in the model gas flow rate leads to a decrease in the number of gas molecules entering the liquid phase interface, thereby reducing both the mass transfer flux and gas removal rate for ethane and *n*-butane within the DES. The mass transfer coefficient and initial mass transfer rate are presented in Table 6, and the fitting results are shown in Table S8. It is shown that decreasing the model gas flow rate results in a slightly reduced mass transfer coefficient and mass transfer rate for both ethane and *n*-butane, which is because lowering the model gas flow rate increases both the thickness of the gas film and liquid film, making it more challenging for gas molecules to diffuse into the liquid phase. Despite these reductions, there is a significant increase in residence time for gases within the DES when using a lower bubbling flow rate, thus indicating a significantly improved dynamic absorption efficiency for VOCs.

https://doi.org/10.1021/acsomega.4c03895
ACS Omega 2024, 9, 30935−30944

Table 5. Mass Transfer Coefficient K_La^0 and Initial Mass Transfer Rate J_0 of Ethane and *n*-Butane in the DES at Different VOC Concentrations

	ethane			*n*-butane		
c_{in} (μmol/mol)	$K_La^0/10^{-3}$ s^{-1}	$J_0/10^{-4}$ mol s^{-1}	R^2	$K_La^0/10^{-3}$ s^{-1}	$J_0/10^{-4}$ mol s^{-1}	R^2
8000	16.96	1.55	0.994	1.67	2.36	0.996
9000	17.05	1.75	0.994	1.69	2.68	0.997
10,000	17.34	1.98	0.995	1.71	3.00	0.997

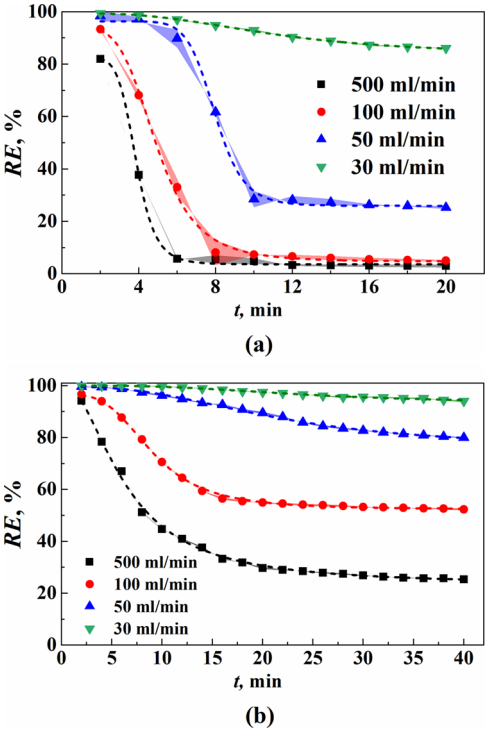

Figure 6. Removal rate of (a) ethane and (b) *n*-butane in the DES at different model gas flow rates.

4.2.4. Influence of Regeneration Times. The recycling performance is an important indicator for evaluating the economic efficiency of an absorbent. Therefore, an investigation was conducted on the dynamic absorption performance with absorption times set at 10, 20, 30, and 40 min of the fresh DES and DES recycled three times. Here, *n*-butane was selected as the representative VOC because of its high content in real oil and gas samples. The results are presented in Figure 7. The dynamic absorption performance of *n*-butane in the recycled solvent was not significantly reduced compared to that in the fresh DES after three cycles of recycling, indicating the excellent regeneration performance of the 1:2 menthol-decanoic acid 1:2 DES.

4.3. Quantum Chemical Calculations. The configurations with the lowest energy were obtained by structure optimization of the ethane, *n*-butane, DL-menthol, decanoic acid, and

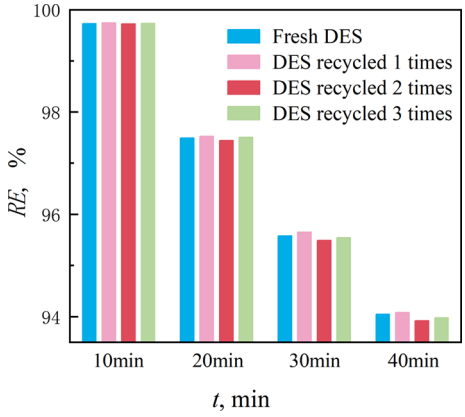

Figure 7. Removal rate of *n*-butane in the DES at different regeneration times.

menthol-decanoic acid 1:2 system. Moreover, no virtual frequency was found through frequency calculations based on the optimized structures, ensuring that the configurations were stable. Molecular interaction energy was calculated based on the optimized configurations, and the results are illustrated in Table 7. The molecular interactions of VOC-DES systems can be classified as weak interactions, indicating that the absorption of VOCs by the DES is a physical process. Considering energy decomposition, the dispersion attraction effect serves as the primary driving force between VOCs and molecules of DES. A strong exchange repulsion effect between VOCs and DES counteracts the weak electrostatic effect. Additionally, it has been observed from the interaction energies between VOC-menthol and VOC-decanoic acid systems that both menthol and decanoic acid significantly impact the interaction between VOCs and DES. The interaction between *n*-butane and DES is much stronger than that of the ethane-DES system, which explains why the solubility of *n*-butane is higher than that of ethane in the DES.

5. CONCLUSIONS

The absorption performance and mechanism of the menthol-decanoic acid 1:2 DES toward ethane and *n*-butane light hydrocarbon VOCs were investigated. Solubility experiments were conducted at 288.2, 293.2, and 298.2 K to investigate the

Table 6. Mass Transfer Coefficient K_La^0 and Initial Mass Transfer Rate J_0 of Ethane and *n*-Butane in the DES at Different Model Gas Flow Rates

	ethane			*n*-butane		
F (mL/min)	$K_La^0/10^{-3}$ s^{-1}	$J_0/10^{-4}$ mol s^{-1}	R^2	$K_La^0/10^{-3}$ s^{-1}	$J_0/10^{-4}$ mol s^{-1}	R^2
500	94.42	10.77	0.998	10.48	18.47	0.998
100	30.72	3.50	0.994	2.43	4.29	0.997
50	17.98	2.05	0.995	1.91	3.38	0.998
30	17.34	1.98	0.995	1.71	3.00	0.997

https://doi.org/10.1021/acsomega.4c03895
ACS Omega 2024, 9, 30935−30944

Table 7. Interaction Energy of VOC-Menthol, VOC-Decanoic Acid, and VOC-DES Systems[a]

		ΔE_{FF}[a] (kJ mol^{-1})				
A	B	E_{ele}	E_{rep}	E_{disp}	ΔE	ΔE_{QC}[b] (kJ mol^{-1})
ethane	DL-menthol	−5.28	13.64	−28.37	−20.01	−22.41
ethane	decanoic acid	−12.63	5.46	−13.76	−20.93	−21.95
ethane	DES	−4.06	25.98	−48.23	−26.31	−28.69
n-butane	DL-menthol	−2.81	18.13	−37.72	−22.40	−27.67
n-butane	decanoic acid	−10.85	11.54	−24.56	−23.87	−26.84
n-butane	DES	−5.71	34.21	−66.39	−37.89	−41.35

[a]ΔE_{FF}[a] and ΔE_{QC}[b] are the interaction energies based on the force field method and quantum chemical calculation, respectively.

absorption performance of the DES toward individual light hydrocarbon VOCs, and the Henry coefficient was determined through fitting. The results revealed that *n*-butane exhibited a higher solubility in the DES compared to ethane. Notably, the solubility of ethane in the DES reached a level comparable to that of an IL, while the solubility of *n*-butane increased by more than 20% than imidazole IL to 0.599 at 298.2 K and 0.101 MPa. Dynamic absorption experiments investigated the influence of the concentration and flow rate of the model gas, temperature, and regeneration times of the DES on the dynamic absorption efficiency. It was demonstrated that as the concentration of VOCs increased and the gas flow rate decreased, the dynamic removal rate of VOCs in the DES increased. The effect of the temperature on the dynamic removal rate was influenced by both a decrease in solubility and an increase in mass transfer rate. The removal rate of *n*-butane reached 99.99% at a temperature of 293.2 K, a VOC concentration of 10,000 μmol/mol, and a gas flow rate of 30 mL/min. Furthermore, the DES could be regenerated by vacuum heating without a significant decrease in its absorption performance after three regeneration cycles when compared with the fresh absorbent, thus indicating its good regeneration performance. The mechanism of light hydrocarbon VOCs absorbed by the DES was revealed through a molecular interaction energy calculation. The results indicate that the butane-DES system exhibits a stronger molecule interaction compared to ethane, thereby resulting in higher absorption performance of *n*-butane by the DES. Moreover, van der Waals interactions, particularly dispersion attractions, serve as the primary attractive forces between light hydrocarbons and DES.

Typically, VOCs in oil products contain light hydrocarbons, which pose challenges in terms of liquefaction and concentration. Currently, there is a lack of efficient methods for the recovery of these light hydrocarbons, thereby impeding the achievement of comprehensive VOC treatment. In this work, the high solubility and dynamic removal rate of light hydrocarbons with the menthol and decanoic acid DES have been proven, making it a promising absorbent with high efficiency for VOC recovery in the petrochemical industry. In the future, further investigation is needed, such as more complex VOC components in the model gas or the real exhaust gas as the research objective to achieve more authentic results that are closer to industrial practice and continuous absorption-regeneration experiments to investigate the long-term absorption efficiency. Additionally, larger-scale experiments are necessary to achieve further industrial applications.

■ ASSOCIATED CONTENT

Supporting Information

The Supporting Information is available free of charge at https://pubs.acs.org/doi/10.1021/acsomega.4c03895.

Equilibrium pressure and liquid phase composition of light hydrocarbons; statistical parameters for the linear fitting Henry's law constant; VOC concentrations at the outlet of the device with different temperatures; statistical parameters for the nonlinear function fitting for different temperatures in the dynamic bubbling experiments; VOC concentrations at the outlet of the device with different intel VOC concentrations; statistical parameters for the nonlinear function fitting for different VOC concentrations of the model gas in the dynamic bubbling experiments; VOC concentrations at the outlet of the device with different flow rates of the model gas; and statistical parameters for the nonlinear function fitting for different flow rates of the model gas in the dynamic bubbling experiments (PDF)

■ AUTHOR INFORMATION

Corresponding Author

Yunfei Song − *State Key Laboratory of Chemical Safety, Qingdao, Shandong 266000, China; SINOPEC Research Institute of Safety Engineering Co., Ltd., Qingdao, Shandong 266000, China;* orcid.org/0009-0004-8879-3945; Phone: +86 19863756171; Email: songyunf.qday@sinopec.com

Complete contact information is available at: https://pubs.acs.org/10.1021/acsomega.4c03895

Notes

The author declares no competing financial interest.

■ ACKNOWLEDGMENTS

This work was supported by the SINOPEC science and technology project (324012). The author is grateful to the editor and the anonymous reviewers.

■ REFERENCES

(1) Li, J.; Hao, Y.; Simayi, M.; Shi, Y.; Xi, Z.; Xie, S. Verification of anthropogenic VOC emission inventory through ambient measurements and satellite retrievals. *Atmospheric Chemistry and Physics* **2019**, *19* (9), 5905−5921.

(2) Gan, G.; Fan, S.; Li, X.; Zhang, Z.; Hao, Z. Adsorption and membrane separation for removal and recovery of volatile organic compounds. *Journal of Environmental Sciences* **2023**, *123*, 96−115.

(3) Wang, J.; Song, Y.; Yin, S.; Shan, X. Simulation study on adsorption and gradation optimization of activated carbon. *Saf. Health Environ.* **2022**, *22* (05), 36−42.

(4) Zhang, C.; Li, K.; Zhang, Y.; Li, G. Status analysis and technical upgrading transform of VOCs recovery unit in refinery. *Chem. Eng. Oil Gas* **2019**, *48* (2), 33−36.

(5) Li, Y.; Chang, H.; Yan, H.; Tian, S.; Jessop, P. G. Reversible absorption of volatile organic compounds by switchable-hydrophilicity

solvents: A case study of toluene with N. *N-Dimethylcyclohexylamine*. *ACS Omega* **2021**, *6*, 253−264.
(6) Berenjian, A.; Chan, N.; Malmiri, H. J. Volatile organic compounds removal methods: A review. *Am. J. Biochem. Biotechnol.* **2012**, *8* (4), 220−229.
(7) Li, Y.; Luo, H. Integration of light hydrocarbons cryogenic separation process in refinery based on LNG cold energy utilization. *Chem. Eng. Res. Des.* **2015**, *93*, 632−639.
(8) Cui, X, Wang, X, Chen, L, Xing, H. Ionic Liquids for Light Hydrocarbon Separation. In *Encyclopedia of Ionic Liquids*; Zhang, S. Eds.; Springer: Singapore, 2022.
(9) Huang, W. Several key issues on oil vapor recovery technology. *Oil Gas Storage Transp.* **2017**, *36* (06), 606−616.
(10) Khan, F. I.; Ghoshal, A. K. Removal of volatile organic compounds from polluted air. *J. Loss Prev. Process Ind.* **2000**, *13* (6), 527−545.
(11) Huang, J.; Zhao, W.; Chen, L.; Wang, Z.; Shi, Y. The application of absorption process for VOCs gases of benzene. *Guangdong Chem. Ind.* **2011**, *38* (11), 79−80.
(12) Quijano, G.; Couvert, A.; Amrane, A.; Darracq, G.; Couriol, C.; Cloirec, P. L.; Paquin, L.; Carrié, D. Potential of ionic liquids for VOC absorption and biodegradation in multiphase systems. *Chem. Eng. Sci.* **2011**, *66* (12), 2707−2712.
(13) Yu, G.; Mu, M.; Li, J.; Wu, B.; Xu, R.; Liu, N.; Chen, B.; Dai, C. Imidazolium-based ionic liquids introduced into π-electron donors: Highly efficient toluene capture. *ACS Sustainable Chem. Eng.* **2020**, *8* (24), 9058−9069.
(14) Zhao, W.; Wu, X.; Li, C.; Lu, C.; Zhang, F. Study on absorption of low pressure acetone vapor in imidazole ionic liquids. *J. Nanjing Univ.* **2017**, *53* (06), 1171−1177.
(15) Gui, C.; Li, G.; Zhu, R.; Liu, Q.; Lei, Z. Ionic liquids for capturing 1,2-dimethoxyethane (DMET) in VOCs: Experiment and mechanism exploration. *Ind. Eng. Chem. Res.* **2022**, *61* (5), 2257−267.
(16) Kurnia, K. A.; Matheswaran, P.; How, C. J.; Noh, M. H.; Kusumawati, Y. A comprehensive study on the impact of chemical structures of ionic liquids on the solubility of ethane. *New J. Chem.* **2020**, *44*, 11155−11163.
(17) Zhang, Y.; Zhao, X.; Yang, Q.; Ren, Q.; Xing, H. Long-chain carboxylate ionic liquids combining high solubility and low viscosity for light hydrocarbon separations. *Ind. Eng. Chem. Res.* **2017**, *56*, 7336−7344.
(18) Liu, X.; Afzal, W.; Prausnitz, J. M. Solubilities of small hydrocarbons in tetrabutylphosphonium bis(2,4,4-trimethylpentyl) phosphinate and in 1-ethyl-3-methylimidazolium bis-(trifluoromethylsulfonyl)imide. *Ind. Eng. Chem. Res.* **2013**, *52* (42), 14975−14978.
(19) Liu, X.; Afzal, W.; Yu, G.; He, M.; Prausnitz, J. M. High solubilities of small hydrocarbons in trihexyl tetradecylphosphonium bis(2,4,4-trimethylpentyl) phosphinate. *J. Phys. Chem. B* **2013**, *117* (36), 10534−10539.
(20) Makino, T.; Kanakubo, M. Absorption of n-butane in imidazolium and phosphonium ionic liquids and application to separation of hydrocarbon gases. *Sep. Purif. Technol.* **2019**, *214*, 139−147.
(21) Afzal, W.; Liu, X.; Prausnitz, J. M. Physical data for a process to separate krypton from air by selective absorption in an ionic liquid. *Fluid Phase Equilib.* **2015**, *404*, 124−130.
(22) Abbott, A. P.; Capper, G.; Davies, D. L.; Rasheed, R. K.; Tambyrajah, V. Novel solvent properties of choline chloride/urea mixtures. *Chem. Commun.* **2003**, *1*, 70−71.
(23) Cheng, Y.; Hu, D.; Xu, Y.; Liu, H.; Lu, H.; Cui, G. Application of ionic liquid-based deep eutectic solvents for CO_2 conversion. *CIESC J.* **2023**, *74* (09), 3640−3653.
(24) Wang, J.; Cheng, H.; Song, Z.; Chen, L.; Deng, L.; Qi, Z. Carbon dioxide solubility in phosphonium-based deep eutectic solvents: An experimental and molecular dynamics study. *Ind. Eng. Chem. Res.* **2019**, *58* (37), 17514−17523.
(25) Alhadid, A.; Safarov, J.; Mokrushina, L.; Müller, K.; Minceva, M. Carbon dioxide solubility in nonionic deep eutectic solvents containing phenolic alcohols. *Front. Chem.* **2022**, *10*, No. 864663.
(26) Haghbakhsh, R.; Raeissi, S. Modeling vapor-liquid equilibria of mixtures of SO_2 and deep eutectic solvents using the CPA-NRTL and CPA-UNIQUAC models. *J. Mol. Liq.* **2018**, *250*, 259−268.
(27) Akhmetshina, A. I.; Petukhov, A. N.; Mechergui, A.; Vorotyntsev, A.; Nyuchev, A. A.; Moskvichev, A.; Vorotyntsev, I. Evaluation of methanesulfonate-based deep eutectic solvent for ammonia sorption. *Journal of Chemical & Engineering Data* **2018**, *63* (6), 1896−1904.
(28) Jin, Z.; Qiu, K.; Liu, X.; Liu, Z.; Liu, L. Experimental research of the efficient oxidation and absorption of H_2S by $CuCl_2$ cooperation with deep eutectic solvent ($FeCl_3$/EG). *Chem. Eng. Oil Gas* **2022**, *51* (6), 8−15.
(29) Moura, L.; Moufawad, T.; Ferreira, M.; Bricout, H.; Tilloy, S.; Monflier, E.; Gomes, M. F. C.; Landy, D.; Fourmentin, S. Deep eutectic solvents as green absorbents of volatile organic pollutants. *Environ. Chem. Lett.* **2017**, *15* (4), 747−753.
(30) Słupek, E.; Makos, P.; Gebicki, J.; Rogala, A. Purification of model biogas from toluene using deep eutectic solvents. *E3S Web Conf.* **2019**, *116*, No. 00078.
(31) Song, Y.; Chen, S.; Luo, F.; Sun, L. Absorption of toluene using deep eutectic solvents: Quantum chemical calculations and experimental investigation. *Ind. Eng. Chem. Res.* **2020**, *59* (52), 22605−22618.
(32) Moufawad, T.; Gomes, M. C.; Fourmentin, S. Deep eutectic solvents as absorbents for VOC and VOC mixtures in static and dynamic processes. *Chem. Eng. J.* **2022**, *448*, No. 137619.
(33) Chen, C. C.; Huang, Y. H.; Hung, S. M.; Chen, C.; Lin, C. W.; Yang, H. H. Hydrophobic deep eutectic solvents as attractive media for low-concentration hydrophobic VOC capture. *Chemical Engineering Journal* **2021**, *424*, No. 130420.
(34) Martins, M. A. R.; Crespo, E. A.; Pontes, P. V. A.; Silva, L. P.; Bülow, M.; Maximo, G. J.; Batista, E. A. C.; Held, C.; Pinho, S. P.; Coutinho, J. A. P. Tunable hydrophobic eutectic solvents based on terpenes and monocarboxylic acids. *ACS Sustainable Chem. Eng.* **2018**, *6* (7), 8836−8846.
(35) Wang, G.; Hou, W.; Xiao, F.; Geng, J.; Wu, Y.; Zhang, Z. Low-viscosity triethylbutylammonium acetate as a task-specific ionic liquid for reversible CO_2 absorption. *Journal of Chemical & Engineering Data* **2011**, *56*, 1125−1133.
(36) Huang, K.; Cai, D.; Chen, Y.; Wu, Y.; Hu, X.; Zhang, Z. Thermodynamic validation of 1-alkyl-3-methylimidazolium carboxylates as task-specific ionic liquids for H_2S absorption. *AIChE J.* **2013**, *59*, 2227−2235.
(37) Li, C.; Gao, K.; Meng, Y.; Wu, X.; Zhang, F.; Wang, Z. Solution thermodynamics of imidazolium-based ionic liquids and volatile organic compounds: Benzene and acetone. *Journal of Chemical & Engineering Data* **2015**, *60*, 1600−1607.
(38) Biard, P. F.; Coudon, A.; Couvert, A.; Giraudet, S. A simple and timesaving method for the mass-transfer assessment of solvents used in physical absorption. *Chemical Engineering Journal* **2016**, *290*, 302−311.
(39) Yu, F.; Wang, F.; Zhang, L.; Zhang, M.; Zhou, L.; Xie, C.; Bao, Y.; Chen, W.; Gong, J. Uncovering dissolution behavior and thermodynamic properties of metronidazole benzoate in twelve mono-solvents by experiments and molecular simulation. *J. Mol. Liq.* **2024**, *393*, No. 123539.
(40) Liu, L.; Hao, X.; Yan, J.; Chen, S. Separation of ethyl acetate-isopropanol using low transition temperature mixtures: Vapor-liquid equilibrium experiments and quantum chemical calculation. *J. Mol. Liq.* **2022**, *367* (Part B), No. 120589.
(41) Neese, F. The ORCA program system—Version 5.0. WIREs Computational Molecular. *Science* **2022**, *12*, No. e1606.
(42) Brandenburg, J. G.; Bannwarth, C.; Hansen, A.; Grimme, S. B97−3c: A revised low-cost variant of the B97-D density functional method. *J. Chem. Phys.* **2018**, *148*, No. 064104.
(43) Lu, T.; Chen, F. Multiwfn: A multifunctional wavefunction analyzer. *J. Comput. Chem.* **2012**, *33* (5), 580−592.

https://doi.org/10.1021/acsomega.4c03895
ACS Omega 2024, 9, 30935−30944

(44) Mortimer, R G. The Molecular Theory of Dilute Gases at Equilibrium, 10-Gas Kinetic Theory. In *Physical Chemistry (Second ed.)*; Mortimer, R. G., Ed.; Academic Press: 2000; pp 319−364.
(45) Evans, R.; Poggetto, G. D.; Nilsson, M.; Morris, G. A. Improving the interpretation of small molecule diffusion coefficients. *Anal. Chem.* **2018**, *90* (6), 3987−3994.
(46) Lewis, W. K.; Whitman, W. G. Principles of gas absorption. *Ind. Eng. Chem. Res.* **1924**, *16*, 1215−1220.
(47) Fick, A. Ueber diffusion. *Annalen der Physik* **1855**, *170* (1), 59−86.

https://doi.org/10.1021/acsomega.4c03895
ACS Omega 2024, 9, 30935−30944